

Robbert Q. Kim,<sup>a,b</sup> Wendy A. Offen,<sup>a</sup> Gideon J. Davies<sup>a\*</sup> and Keith A. Stubbs<sup>c</sup>

<sup>a</sup>York Structural Biology Laboratory, Department of Chemistry, University of York, York YO10 5DD, England, <sup>b</sup>Division of Biochemistry, The Netherlands Cancer Institute, Plesmanlaan 121, 1066 CX Amsterdam, The Netherlands, and <sup>c</sup>School of Chemistry and Biochemistry, University of Western Australia, 35 Stirling Highway, Crawley, Western Australia 6009, Australia

Correspondence e-mail:  
gideon.davies@york.ac.uk

# Structural enzymology of *Helicobacter pylori* methylthioadenosine nucleosidase in the futasosine pathway

The recently discovered futasosine pathway is a promising target for the development of new antibiotics. The enzymes involved in this pathway are crucial for the biosynthesis of the essential prokaryotic respiratory compound menaquinone, and as the pathway is limited to few bacterial species such as the gastric pathogen *Helicobacter pylori* it is a potential target for specific antibiotics. In this report, the crystal structure of an *H. pylori* methylthioadenosine nucleosidase (MTAN; an enzyme with broad specificity and activity towards 6-amino-6-deoxyfutasosine), which is involved in the second step of menaquinone biosynthesis, has been elucidated at a resolution of 1.76 Å and refined with  $R$  factors of  $R_{\text{work}} = 17\%$  and  $R_{\text{free}} = 21\%$ . Activity studies on the wild type and active-site mutants show that the hydrolysis of 6-amino-6-deoxyfutasosine follows a mechanism similar to that of *Escherichia coli* MTAN. Further evidence for this mode of action is supplied by the crystal structures of active-site mutants. Through the use of reaction intermediates, the structures give additional evidence for the previously proposed nucleosidase mechanism. These structures and the confirmed reaction mechanism will provide a structural basis for the design of new inhibitors targeting the futasosine pathway.

Received 28 August 2013  
Accepted 26 September 2013

**PDB references:** HpyMqnB, 4bmx; E14Q mutant, 4bn0; D199N mutant, 4bmz; D199A mutant, 4bmy

## 1. Introduction

The discovery of penicillin in 1928 is considered to be a landmark in the fight against bacterial infections. During the rest of the twentieth century the development of a range of new antibiotics was achieved; however, during the latter few decades the rate of discovery of new antibiotics decreased significantly (Nathan, 2004). The development of antibiotics has focused mainly on enzymes involved in one of four bacterial processes: protein, nucleic acid and cell-wall synthesis, and folate metabolism (as reviewed by Walsh, 2003 and Kohanski *et al.*, 2010). These cellular pathway targets are well conserved in many bacterial strains; therefore, compounds which are developed by classical synthetic and library methods are effective against a range of species. Unfortunately, the specific focus on these pathways has led to an increased rate of antibiotic resistance, and thus new targets which have not had selective pressures placed on them are desperately needed (see the review by Sommer & Dantas, 2011). In order to investigate possible antimicrobial compounds through rational drug design, more (structural) knowledge about a targeted pathway is ideal.

A key molecule in the bacterial respiratory pathway is menaquinone, a lipid-soluble electron carrier known in eukaryotes as vitamin K<sub>2</sub> (Suttie, 1995). It is the only known electron transporter in Gram-positive bacteria and is also used

during anaerobic growth in Gram-negative strains. Humans lack a biosynthesis pathway for vitamin K<sub>2</sub>, which makes the menaquinone biosynthetic pathway a potential target for antibacterial design (Kurosu & Begari, 2010; Fig. 1). The enzymes involved in menaquinone biosynthesis have been identified in various strains (Glasner *et al.*, 2006) and the pathway and its intermediate compounds have been described for the model organism *Escherichia coli* (Bentley & Megathathan, 1982).

Intriguingly, not all bacteria utilize the same pathway for the biosynthesis of menaquinone. Although organisms such as *Helicobacter pylori*, *Thermus thermophilus* and *Streptomyces coelicolor* use menaquinone and chorismate, no *men* homologues have been found and they appear to lack the conventional menaquinone biosynthetic machinery (Borodina *et al.*, 2005). Further studies support this, as these organisms have been shown to produce other intermediates during menaquinone synthesis (Seto *et al.*, 2008). Analysis of the genome of *S. coelicolor* using *BLAST* and comparison to microorganisms exhibiting the characterized menaquinone biosynthetic pathway resulted in the identification of candidate genes involved in a new pathway termed the ‘futalosine pathway’ (Hiratsuka *et al.*, 2008). Disruption experiments on these genes provided evidence of their involvement in the futalosine pathway as well as an indication of their consecution in the pathway. The order of involvement of the relevant gene products was further demonstrated by analysis of the intermediate compounds (Seto *et al.*, 2008; Hiratsuka *et al.*, 2009), allowing a more complete picture of the futalosine pathway (Fig. 1), and resulted in the renaming of the gene products MqnA, MqnB, MqnC and MqnD, respectively. MqnA is thought to use adenosine and the common branch-point material chorismate (1) to produce 6-amino-6-deoxyfutalosine (11). The next step involves the hydrolysis of this product by

MqnB to form adenine and dehydropoxanthinyl futalosine (13); the latter is then cyclized by MqnC to give (14) before being processed by MqnD. The product of the reaction catalyzed by MqnD, 1,4-dihydroxy-6-naphthoic acid (15), undergoes further modifications to ultimately yield menaquinone (10) carried out by the putative enzymes MqnE to MqnH. These presumably mediate the decarboxylation, prenylation and methylation of (15) (Seto *et al.*, 2008; Tanaka *et al.*, 2011), although none of these steps have been biochemically characterized to date.

Interestingly, a divergence within the futalosine pathway has also been found (Arakawa *et al.*, 2011). Analysis of the second step in the futalosine pathway revealed differences in substrate specificity for the hydrolase MqnB. In *H. pylori* and *Campylobacter jejuni* it was shown that MqnB (HpyMqnB and CjjMqnB, respectively) processes 6-amino-6-deoxyfutalosine (11) as a substrate (Li *et al.*, 2011), but is unable to utilize futalosine (12). Homologues from *Acidothermus cellulosycticus* and *T. thermophilus*, however, showed the opposite activity, which has also been proposed for *S. coelicolor* (Arakawa *et al.*, 2011). The two substrates only differ slightly in their nucleoside groups, where the base is hypoxanthine in compound (12) and adenine in compound (11), and this underlines the narrow specificity of these enzymes (Fig. 1).

HpyMqnB is listed as a 5'-methylthioadenosine/S-adenosylhomocysteine nucleosidase (MTAN) and the structure of the enzyme has recently been published in classic work by Ronning and coworkers (PDB entry 3nm4; Ronning *et al.*, 2010). The MTAN has been shown to process other substrates (Ronning *et al.*, 2010) and is involved in salvage pathways (Zhao *et al.*, 2003; Albers, 2009). These results suggest that the specificity of the enzyme encompasses the adenosine moiety; structural alignment with the *S. coelicolor* homologue (Fig. 2), which processes futalosine (12), indicates that an aspartic acid

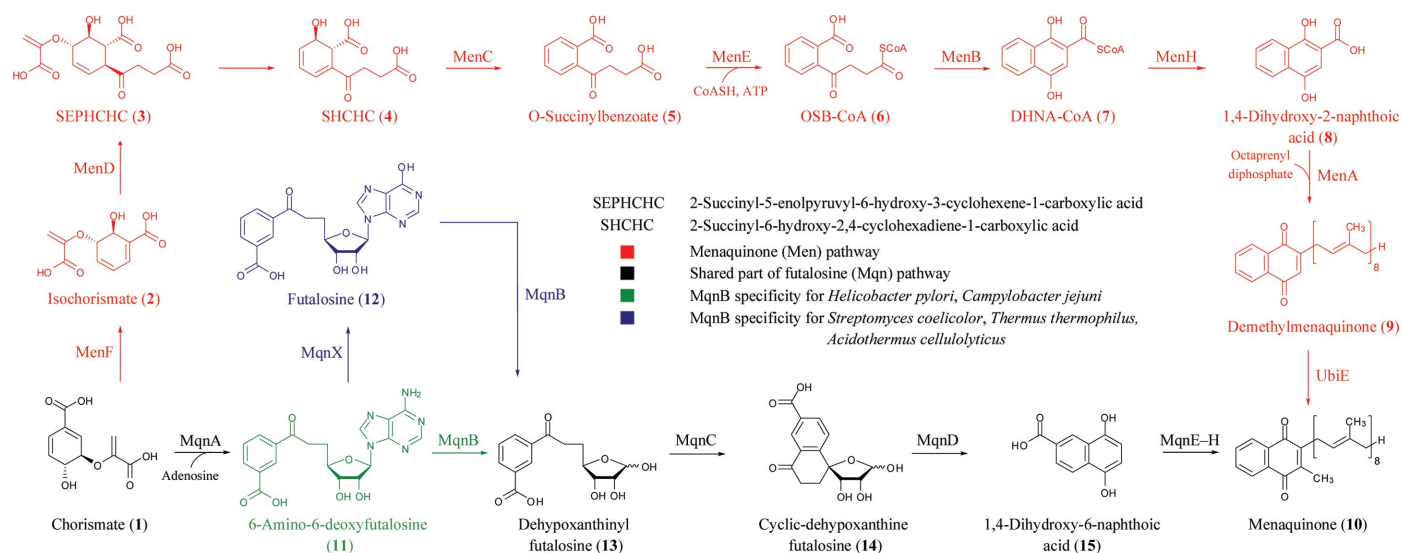


**Figure 1**  
The menaquinone pathway found in various species such as *E. coli* uses eight enzymes: MenA–MenH (coloured red). The newly found futalosine pathway uses Mqn enzymes to synthesize menaquinone (shown in black). A small divergence has been found for MqnB: species such as *H. pylori* and *C. jejuni* use 6-amino-6-deoxyfutalosine as a substrate (green), whereas *S. coelicolor*, *T. thermophilus* and *A. cellulosycticus* use the deaminase MqnX (blue) to process futalosine.

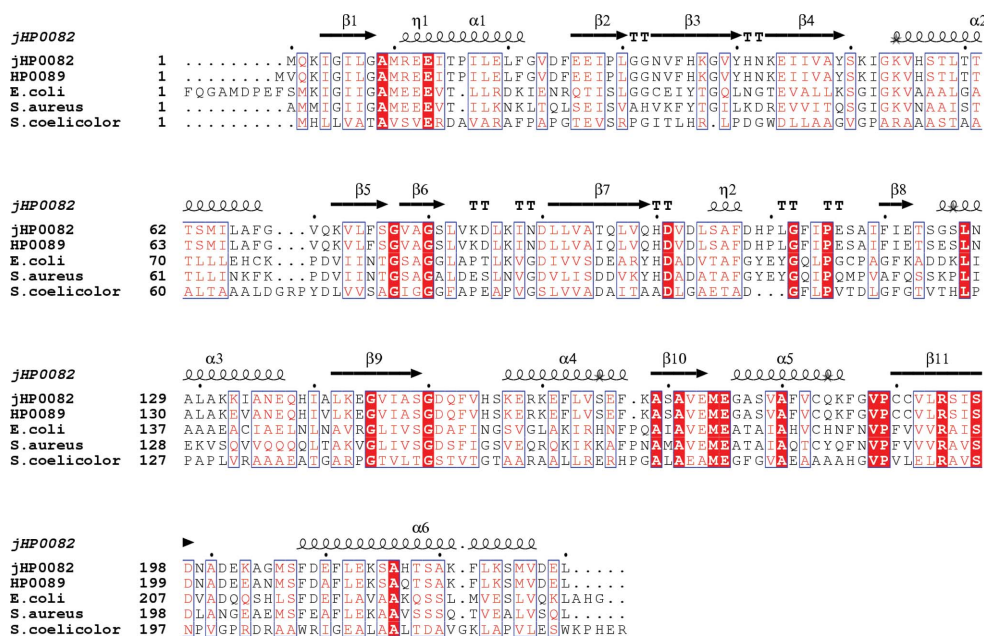


**Figure 2**  
The sequence of HpyMqnB (HP0089) aligned with homologous MTANs with known three-dimensional structures and the futalosine hydrolase from *S. coelicolor*. Conserved residues are shown on a red background and similar regions are boxed in blue. The secondary structure of the *H. pylori* enzyme (jHP0082) is depicted above the alignment. This figure was created using *ESPrpt* (Gouet *et al.*, 2003).

in the active site (Asp198) potentially plays a major role in this nucleoside specificity. This subtle change in the active substrate underlines the importance of MqnB and gives it potential as a new antibiotic target; it is especially of interest that a potent inhibitor of HpyMqnB has recently been developed (Wang *et al.*, 2012), alongside those for the *E. coli* homologue (Singh *et al.*, 2005).

In this study, we present the structure of HpyMqnB and through the use of structural biochemical analysis confirm the mechanism of the enzyme and show that it is closely related to *E. coli* methylthioadenosine nucleosidase (MTAN; Lee *et al.*, 2001b, 2003; Lee, Singh *et al.*, 2005), despite its low overall sequence homology of 30%. Evidence for the role of critical residues in the active site is also provided by the crystal structures of active site mutants, further supporting the proposed mechanism for the hydrolysis of adenosine-containing compounds such as methylthioadenosine (MTA).

## 2. Materials and methods

### 2.1. Chemicals and molecular-biology agents

Chemicals were purchased from Sigma–Aldrich unless stated otherwise. The substrate 6-amino-6-deoxyfutalosine was synthesized according to the literature (Arakawa *et al.*, 2011). Primers were ordered through Eurofins MWG Operon, Ebersberg, Germany.

### 2.2. Development of (mutant) methylthioadenosine nucleosidases

The wild-type MTAN gene from *H. pylori* strain 26695 (HpyMqnB) was synthesized in a form codon-optimized for

*E. coli* expression by GenScript and was ligated into a pET-28 expression vector (Novagen) containing a cleavable N-terminal hexahistidine tag. Site-directed mutagenesis was performed using the QuikChange protocol (Stratagene) or the overhang method proposed by Liu & Naismith (2008) to obtain the active-site mutants. For high GC-content targets, the PCR mixture was supplemented with 2.2 M betaine (Baskaran *et al.*, 1996). After amplification, the original DNA was digested with *DpnI* for 2 h at 37°C and cleaned up with the Promega PCR Clean-Up system. The resulting DNA was transformed into XL10 Gold cells (Agilent) and amplified by overnight growth of the bacteria in Luria–Bertani (LB) medium at 37°C. The DNA was isolated with a Miniprep Kit (Qiagen) and sequenced to confirm the mutation.

### 2.3. Protein production and purification

The wild-type and mutant plasmids were transformed into *E. coli* BL21 (DE3) cells and grown in 5 ml LB medium supplemented with 50 µg l<sup>-1</sup> kanamycin for 2 h at 37°C. The preculture was added to 800 ml LB with antibiotic and grown at 37°C until the OD<sub>600</sub> reached 0.6. The culture was then induced with 1 mM isopropyl β-D-1-thiogalactopyranoside (IPTG) and shaken at 180 rev min<sup>-1</sup> for 16–20 h at 16°C. The bacteria were harvested by centrifugation, resuspended in buffer A (50 mM Tris–HCl pH 8.0, 500 mM NaCl, 20 mM imidazole) and stored at –20°C until use.

On thawing, the cells were lysed by ten cycles of 12 s of sonication and the insoluble matter was pelleted by centrifugation for 25 min. The supernatant was applied onto a 1 ml HisTrap column (GE Healthcare) pre-equilibrated with buffer

**Table 1**

Data-processing and refinement statistics for the crystal structures of HpyMqnB and mutants.

Values in parentheses are for the outer resolution shell.

	Wild type	E14Q	D199N	D199A
PDB code	4bmx	4bn0	4bmz	4bmy
Space group	$P2_12_12_1$	$P2_1$	$I2$	$C222_1$
Unit-cell parameters				
$a$ (Å)	59.31	64.23	67.44	54.85
$b$ (Å)	90.57	75.69	67.75	123.4
$c$ (Å)	108.4	97.01	100.1	145.9
$\alpha$ (°)	90	90	90	90
$\beta$ (°)	90	106.4	105	90
$\gamma$ (°)	90	90	90	90
Monomers in asymmetric unit	2	4	2	2
Resolution (Å)	54.19–1.76 (1.79–1.76)	39.64–2.11 (2.17–2.11)	55.48–1.79 (1.83–1.79)	56.83–1.65 (1.68–1.65)
Beamline	I02, DLS	I04-1, DLS	I04-1, DLS	I04-1, DLS
Wavelength (Å)	0.979	0.9163	0.9163	0.9163
Observed reflections	577503 (24351)	171168 (14755)	168423 (11126)	488111 (22847)
Unique reflections	57414 (3232)	48788 (4099)	40405 (2612)	59812 (2896)
$R_{\text{merge}}$	0.130 (0.92)	0.132 (0.46)	0.046 (0.62)	0.077 (0.87)
Multiplicity	10.1 (7.5)	3.5 (3.6)	4.2 (4.3)	8.2 (7.9)
Completeness (%)	98.0 (96.9)	95.1 (98.0)	98.4 (99.0)	99.9 (99.6)
Mean $I/\sigma(I)$	15.8 (2.2)	4.9 (2.1)	15.8 (2.0)	16.9 (2.1)
No. of protein atoms	3515	6689	3465	3428
No. of water molecules	363	165	204	417
No. of ligand/ion atoms	26	0	40	5
$R_{\text{work}}$	0.17	0.27	0.18	0.179
$R_{\text{free}}$	0.21	0.26	0.22	0.20
R.m.s.d. from ideality				
Bond lengths (Å)	0.020	0.016	0.018	0.010
Bond angles (°)	1.986	1.718	1.843	1.950
Chiral volumes (Å <sup>3</sup> )	0.162	0.100	0.132	0.118
Ramachandran plot				
Favoured (%)	96.9	96.5	96.1	97.5
Disallowed (%)	0	0.2	0.4	0
Average $B$ values (Å <sup>2</sup> )				
Protein	20	29	29	20
Waters	29	20	31	29
Ligand/ion	28	—	25	33

$A$  and the protein was eluted with an imidazole gradient. The protein was concentrated and buffer-exchanged into buffer  $C$  (10 mM Tris–HCl pH 8.0). The protein was checked for homogeneity by SDS–PAGE and when necessary was further purified on a Superdex 75 gel-filtration column pre-equilibrated with buffer  $C$ . The production and purification was identical for the wild-type protein and mutants. The molecular weight was confirmed using electrospray mass spectrometry.

#### 2.4. Crystallization, data acquisition and processing

Wild-type and mutants of HpyMqnB were concentrated to 50 mg ml<sup>-1</sup> (measured using a spectrophotometer at 280 nm with an extinction coefficient of 2980 M<sup>-1</sup> cm<sup>-1</sup>) prior to crystallization. Crystals of wild-type HpyMqnB were grown in sitting drops over 4.0 M NaH<sub>2</sub>PO<sub>4</sub>/K<sub>2</sub>HPO<sub>4</sub> pH 7.0 using a 1:1 ratio of protein to mother liquor and were flash-cooled in liquid N<sub>2</sub> without the need for additional cryoprotectant. X-ray diffraction data were obtained from a single crystal on beamline I02 at the Diamond Light Source (DLS), Oxford, England to 1.7 Å resolution. The crystal belonged to space group  $P2_12_12_1$  and the images were processed using *iMosflm* (Leslie & Powell, 2007). Data-processing statistics are shown

in Table 1; the highest resolution was determined by  $I/\sigma(I) > 2.0$ .

The structure of HpyMqnB was solved by molecular replacement using *MOLREP* (Vagin & Teplyakov, 2010) from the *CCP4* suite (Winn *et al.*, 2011). Chain  $A$  of the structure of 5'-methylthioadenosine nucleosidase (PDB entry 3nm4; 95% identity; Ronning *et al.*, 2010) was used as a search model and two monomers were found in the asymmetric unit. The model underwent iterative cycles of maximum-likelihood restrained refinement using *REFMAC5* (Murshudov *et al.*, 2011) and model optimization in *Coot* (Emsley *et al.*, 2010), followed by validation using *PDB\_REDO* (Joosten *et al.*, 2012). The electron density for the final model showed 363 waters, an adenine molecule and two tris(hydroxymethyl)amino-methane (Tris) molecules next to the two protomers.

Crystals were obtained of the HpyMqnB mutants E14Q (0.1 M HEPES pH 7.5, 25% PEG 3350, 0.2 M NaCl), D199N (0.1 M bis-tris pH 5.5, 25% PEG 3350, 0.2 M MgCl<sub>2</sub>·6H<sub>2</sub>O) and D199A (0.1 M bis-tris pH 6.5, 25% PEG 3350, 0.2 M Li<sub>2</sub>SO<sub>4</sub>·H<sub>2</sub>O) and were flash-cooled in liquid N<sub>2</sub>. Data for these crystals were acquired on beamline I04-1 at DLS and were processed with *XDS* (Kabsch, 2010) or *MOSFLM*

(Leslie & Powell, 2007). The structures were solved with *MOLREP* (Vagin & Teplyakov, 2010) using the wild-type structure as a search model. Iterative model building and refinement using *Coot*, *REFMAC* and *PDB\_REDO* (Emsley *et al.*, 2010; Murshudov *et al.*, 2011; Joosten *et al.*, 2012) yielded optimized models with statistics displayed in Table 1.

#### 2.5. <sup>1</sup>H NMR activity assays of 6-amino-6-deoxyfutasoline hydrolysis

Substrate stock solutions were prepared by diluting lyophilized 6-amino-6-deoxyfutasoline in D<sub>2</sub>O to a concentration of 2 mM. The HpyMqnB stocks were prepared at concentrations of approximately 6 mg ml<sup>-1</sup> in 10 mM imidazole pH 7.0. Samples were prepared by adding 150 µl enzyme stock to an Eppendorf tube containing 150 µl substrate and 300 µl D<sub>2</sub>O, giving a final volume of 600 µl. After mixing, the samples were transferred into an NMR tube. <sup>1</sup>H NMR spectra of the samples were recorded at various time points using a TXI probe on a Bruker 700 MHz spectrometer at 298 K. Control reactions containing buffer instead of enzyme showed no spectral changes over the course of several days.

### 3. Results

#### 3.1. Structure of HpyMqnB

The wild-type MTAN from *H. pylori* strain 26695 (HpyMqnB) crystallized in the orthorhombic space group  $P2_12_12_1$ , with unit-cell parameters  $a = 59.3$ ,  $b = 90.6$ ,  $c = 108.4$  Å,  $\alpha = \beta = \gamma = 90^\circ$  (Table 1). The structure contained two protein molecules per asymmetric unit and was determined to a resolution of 1.76 Å with crystallographic  $R$  and  $R_{\text{free}}$  values of 0.17 and 0.21, respectively. The model was obtained by molecular replacement using a search model (PDB entry 3nm4; Ronning *et al.*, 2010) with 95% sequence identity. The refined final model comprised a homodimer (similar to that of Ronning *et al.*, 2010) with 3554 protein atoms, 26 ligand atoms and 414 water molecules. The enzyme was crystallized with a His<sub>6</sub> purification tag which added 20 residues to the chain and which could partly be seen in the electron-density map.

The subunits in the crystal structure of HpyMqnB exhibit a Rossmann fold; they show a slightly curved  $\beta$ -sheet as a core surrounded by six  $\alpha$ -helices (Fig. 3*a*). Although most homologous structures show identical subunits, the *H. pylori* enzyme crystallizes as a dimer with two different states. The main differences between these two forms of the protomer arise because molecule *B* has ligands bound in the active site, whereas molecule *A* has an unoccupied active site with an open conformation. The C-terminal helix ( $\alpha_6$ ) shows a slight kink and the preceding loop forms a cap over the active site in molecule *B*. In the open form of the enzyme, however, the kink and loop relax into a flexible region and no electron density is observed for a substrate. The same was observed in the structure of MqnB from *H. pylori* strain J99 (Ronning *et al.*, 2010), making this the first nucleosidase to crystallize as a dimer with two different forms of the protomer.

Corresponding to the oligomerization state in the crystal, the enzyme migrated as a dimer on a size-exclusion column (data not shown), which indicated a stable dimer in solution. In the crystal structure, the interface of the homodimer is formed by  $\alpha$ -helices  $\alpha_2$  and  $\alpha_5$  and a loop comprising residues 102–127. The dimer interface of roughly 1600 Å<sup>2</sup> indicates a biological cause of complex formation rather than a crystallographic one (Krissinel & Henrick, 2007). Furthermore, the loop interacts directly with amino acids that make up the active site (Fig. 3*a*). This interaction could indicate an allosteric effect, but no evidence for this has been found to date.

The structures of previously solved homologous enzymes (Fig. 2) all show a homodimer in which both partners of the biologically active dimer have the same conformation (Lee *et al.*, 2001*a*; Siu, Lee, Smith *et al.*, 2008; Siu, Lee, Sufrin *et al.*, 2008). The best-studied enzyme in this class, *E. coli* MTAN, has structures with various ligands in the active site, but they always feature a dimer with two protomers in the same state. Comparison of the structure reported here with either the open or ligand-bound state of the *E. coli* structure did not result in any large unexpected differences. Although their sequence identity does not exceed 35%, secondary-structure matching (SSM) shows alignment with a root-mean-square difference (r.m.s.d.) of 1.35 Å between the C $^\alpha$  atoms. The main

difference is in the position of helix  $\alpha_3$ ; however, the residues implicated in enzymatic activity are conserved and align well with those of *E. coli* MTAN.

#### 3.2. Active-site identification

Superposition of corresponding residues of the two subunits yields an r.m.s.d. of 1.24 Å. Upon closer inspection of the two structures, however, this value seems to be mainly derived from differences near the active site. Chain *B* has extra electron density for an adenine and a Tris molecule in the active site (Fig. 3*b*). The presence of these ligands seems to be the cause of this deviation. Both molecules may have bound during protein production, but adenine could also be a remnant of an endogenous adenosine-like substrate processed by the enzyme. The presence of Tris in the active site could be detrimental to activity assays; it has been shown to inhibit homologues (Siu, Lee, Sufrin *et al.*, 2008). The molecule can mimic the transition state for glycoside hydrolysis of a sugar group with its hydroxymethyl arms (Gloster & Davies, 2010) and resembles the ribose moiety of the substrate of HpyMqnB. The residues surrounding this Tris molecule are therefore

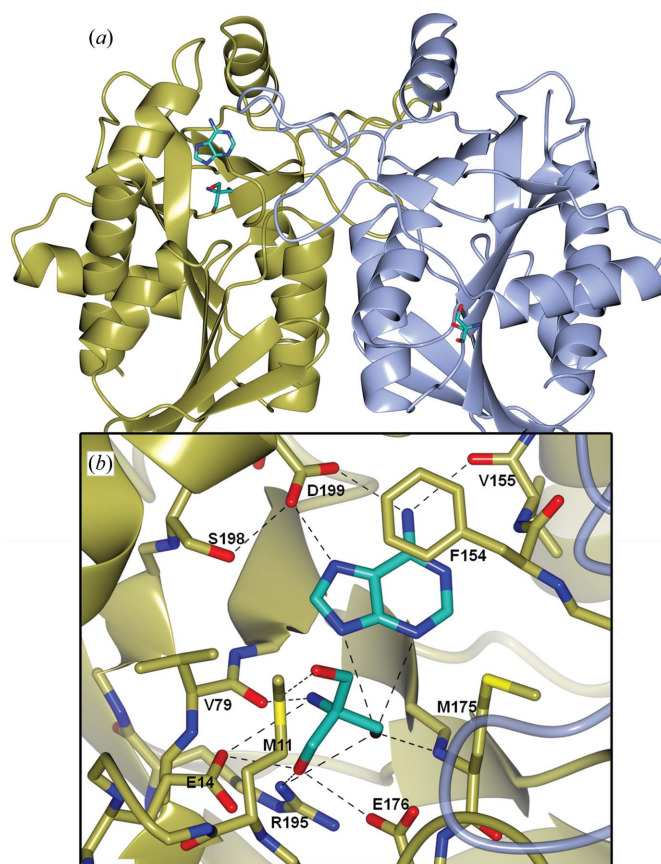


**Figure 3**

The overall structure of HpyMqnB (*a*) shows both an open form (ice blue) and a ligand-bound form (gold) dimerized through two  $\alpha$ -helices and a loop. The interacting loop could have an allosteric effect as its residues are close to the active site, which contains an adenine and a Tris molecule which interact by a hydrogen-bonding network (*b*). Figures were produced using CCP4MG (McNicholas *et al.*, 2011).

likely to play an important role in accommodating the sugar group of the substrates of HpyMqnB.

The Tris molecule is stabilized in the structure by hydrogen bonds to the carboxyl groups of Glu14, Glu174 and Glu176, the guanidinium group of Arg195 and the backbone N atom and carbonyl O atom of Met175 and Val79, respectively (Fig. 3*b*). The carbonyl O atom of Val79 also stabilizes the adenine molecule through a hydrogen bond to N7. The nitrogenous base is further coordinated through ring stacking with Phe154 and hydrogen bonding to the carboxylic side chain of Asp199 and the backbone of Val155. The involvement of these residues in the active site is evident when comparing the open and closed states of the protein. Upon binding of the ligand, the side chain of Glu14 shifts 2.5 Å as helix  $\alpha$ 1 extends further into the active site. Furthermore, Arg195 moves further towards the ligand binding site. As Arg195 and Asp199 interact with the substrate, the unstructured region (residues 201–207) becomes a structured cap over the active site. This conformational change is illustrated by the displacement of residues surrounding this region: helix  $\alpha$ 6 becomes extended (slightly kinked) over the ligand in the binding pocket.

The active site of HpyMqnB is comparable with those of its known homologues, with residues responsible for binding the substrate conserved between various species. MTAN from *E. coli* has been well studied and the active site residues are conserved; HpyMqnB may adopt an enzymatic mechanism (Fig. 4) similar to that proposed for MTAN (Lee, Smith *et al.*, 2005). Substrate binding would involve the hydrogen bonding of Asp199 to the purine group, with support from the adjacent hydroxyl group of Ser198. This binding would tether the adenine moiety, thereby making the bond between N9 and C1 of the ribose more susceptible to nucleophilic attack by a water molecule that is coordinated in the active site by Glu14 and Arg195. Interaction with these residues would activate the water, allowing it to perform the attack and break the bond between the adenine and ribose moiety.

### 3.3. Active-site mutants

To assess whether this model based on the methylthioadenosinase activity of *E. coli* holds true for HpyMqnB and whether the proposed active site residues are essential for the processing of 6-amino-6-deoxyfutalosine, single site-directed mutants were cloned. To render the enzyme potentially unable to bind a ligand, the essential residues Asp199 (which forms hydrogen bonds

to the purine group of the substrate) and Glu14 (the putative base) were mutated to either alanine or the respective amide. The E14Q mutant should be unable to activate the water molecule for nucleophilic attack and the D199N mutation should change the affinity of the enzyme for the adenine moiety of the substrate. Interestingly, the latter mutant mimics the putative active-site residue of the *S. coelicolor* homologue (Fig. 2). This organism also uses the futalosine pathway, but uses futalosine instead of 6-amino-6-deoxyfutalosine as a substrate for MqnB (Fig. 1). The compounds differ by having an O atom instead of an N atom at the purine group which is hydrogen bonded by the aspartic acid in HpyMqnB. Mutating Asp199 to asparagine might confer the ability to process futalosine, as the residue would presumably be able to form hydrogen bonds similar to those of native HpyMqnB and its substrate. Structural and kinetic assessment of the D199N mutant could therefore yield additional clues about the difference in substrate specificity between the *H. pylori* and *S. coelicolor* homologues.

The hydrolase activity of HpyMqnB and its mutants towards 6-amino-6-deoxyfutalosine was tested using  $^1\text{H}$  NMR spectroscopy. Processing 6-amino-6-deoxyfutalosine causes the bond between the adenine and ribose moieties to break,

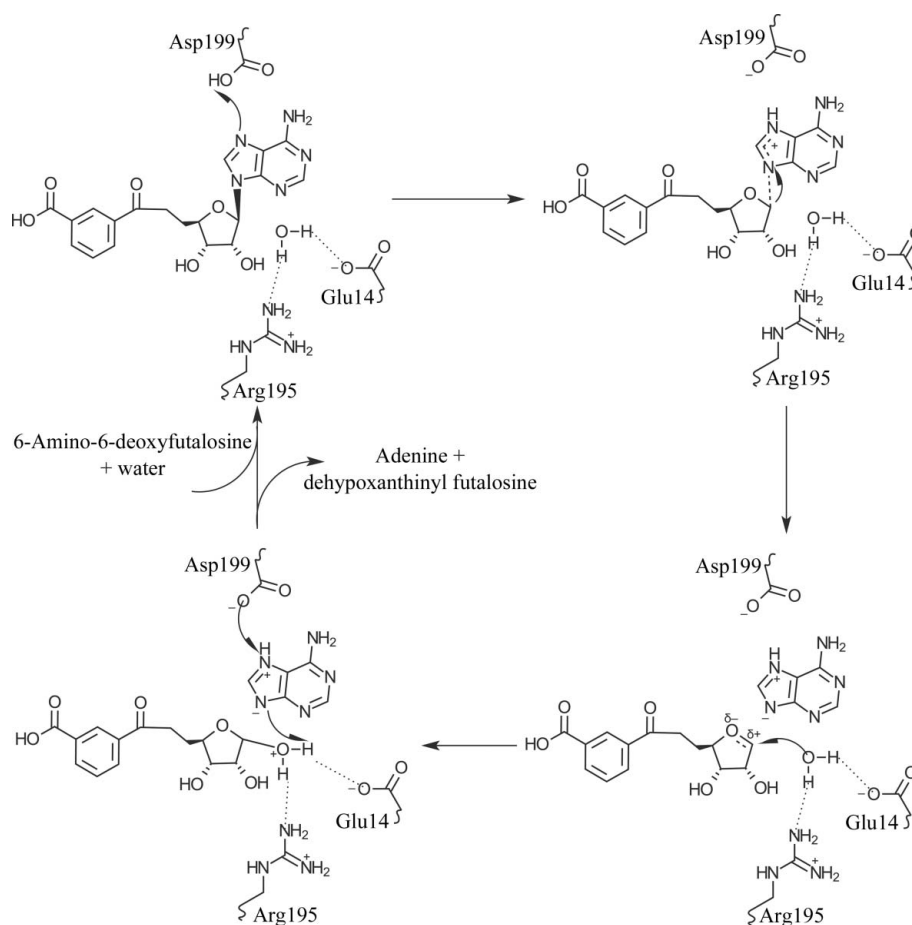


**Figure 4** The proposed mechanism of action for the hydrolysis of MTA by MTANs involves the essential acidic residue in the lid of the active site and a water molecule that acts as a nucleophile which is activated by an arginine and a glutamic acid residue.

yielding adenine and dehydropyranthynyl fufalose. NMR analysis of the enzyme-catalyzed hydrolysis of 6-amino-6-deoxyfufalose (Fig. 5) clearly demonstrated turnover of the substrate by the enzyme. At the initial concentration used, all of the 6-amino-6-deoxyfufalose was processed within 5 min (Fig. 5a) by wild-type HpyMqnB. Even when a 100-fold dilution of the enzyme was used, the substrate peaks were still present in the  $^1\text{H}$  NMR spectrum after 5 min. The catalytic mechanism was probed further by performing an experiment utilizing a low concentration of enzyme (1000-fold dilution). This demonstrated an initial signal at 5.1 p.p.m. corresponding to the  $\alpha$ -anomer and showed the appearance of an additional signal over time corresponding to the  $\beta$ -anomer. This was observed owing to the mutarotation of the product hemiacetal, with the final equilibrium ratio being 65:35 ( $\alpha$ : $\beta$ ), and is consistent with observations for other nucleosidases of this type in terms of these enzymes having an inverting catalytic mechanism (Lee *et al.*, 2003). For the mutant enzymes, however, no product formation was detected after 5 min at the original concentration of 6 mg ml $^{-1}$ . The experiments for the E14Q and D199N mutants showed some product formation over extended periods (4 h; Fig. 5b). This could have arisen from spontaneous hydrolysis aided by the remaining ability of the enzyme to bind the substrate. The mutations do not interfere with the geometry of the active site and substrate binding is still achieved. Once bound to the enzyme the adenine-ribose bond is more susceptible to attack by a water molecule, which ultimately yields hydrolysis products, albeit several orders of magnitude more slowly. The alanine mutants, however, underwent no substrate processing after 4 h, suggesting that these mutations drastically reduce the catalytic activity.

### 3.4. The mutant structures give insight into the mechanism

Further insights into the basis for the inactivity of the mutants were found in the crystal structures of the mutant enzymes. Diffracting crystals were obtained for the E14Q mutant and both Asp199 mutants, albeit in different conditions to those of wild-type HpyMqnB. The crystals belonged to different space groups (Table 1) and the structures were determined by molecular replacement using the wild-type enzyme as a search model. Although the number of molecules in the asymmetric unit varies, the mutants occur as homodimers, similar to the native structure. The main difference, however, is the homogeneity in the dimers: the mutant subunits contain only one state, open or ligand-bound, whereas the wild-type structure exhibits both in the dimer.

In the D199A and E14Q mutants both subunits are in the open form of the enzyme. Therefore, they compare best with the open form of the native enzyme (molecule A): the active site is empty and the capping loop is absent in the electron-density map. The similarity is demonstrated by r.m.s.d. values of 0.35 Å or lower when superposing the open forms of the molecule using SSM. The largest deviations are, unsurprisingly, observed near the mutated residues, providing evidence for alterations in the geometry of the active site. The absence

of an endogenous ligand in the active site, despite similar purification procedures, provides further evidence that the mutants are unable to (tightly) bind the substrate, as confirmed by the abrogated activity demonstrated by the  $^1\text{H}$  NMR experiments. Although there is no ligand bound in the crystal structure of the E14Q mutant, the enzyme still shows minor activity towards 6-amino-6-deoxyfufalose in the NMR experiments. This could be due to the higher amounts of available ligand in the latter experiment. Furthermore, the co-crystallized ligands in the ligand-bound form, which were obtained from the cell lysate, are unable to remain bound during purification if the binding constant is too low.

Interestingly, the D199N mutant does have substrate bound in the crystal structure. This results in a closed form being observed in both subunits of the dimer, corresponding to the ligand-bound form in the wild-type crystal structure. With an r.m.s.d. value of 0.31 Å when superposing the C $^{\alpha}$  atoms, there is very little difference between the two protomers apart from the observed ligand density. Whereas the wild type contains a (presumably processed) ligand, the D199N mutant structure

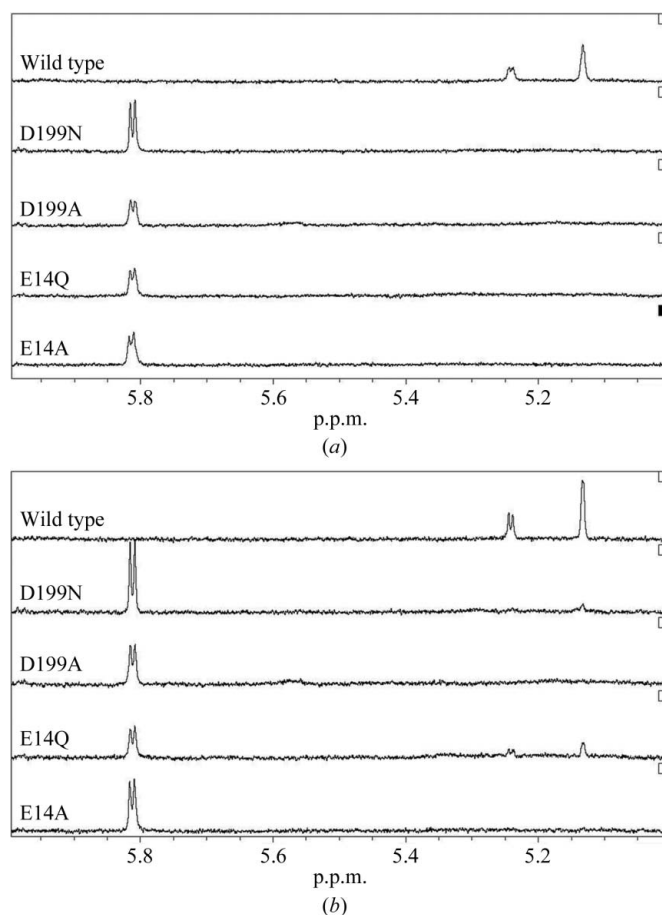


**Figure 5**  
The activity of HpyMqnB and its described mutants towards 6-amino-6-deoxyfufalose. The  $^1\text{H}$  NMR spectra after 5 min (a) show complete hydrolysis for the wild-type enzyme, resulting in two peaks (representing the  $\alpha$ -anomer and the  $\beta$ -anomer). However, the mutants show no (D199A and E14A) or highly reduced (D199N and E14Q) activity even after 4 h (b).

shows density, quite fortuitously, for an unprocessed substrate methylthioadenosine (MTA; Fig. 6*a*). This compound will have been scavenged from the expression host lysate owing to the affinity of the enzyme for the purine moiety. In wild-type HpyMqnB the substrate is actively processed, resulting in the adenine reaction product being observed, while the mutant, with its diminished activity, retains the intact substrate molecule. This intermediate in the reaction mechanism of the enzyme gives insight into the substrate binding, demonstrating the high affinity that HpyMqnB has for methylthioadenosine and providing evidence for the mechanism proposed previously (Ronning *et al.*, 2010).

## 4. Discussion

### 4.1. The structural information further establishes the mode of action

The crystal structures reported here provide a basis for modelling 6-amino-6-deoxyfutalosine in the HpyMqnB substrate-binding site. The substrate has an isophthalic acid at C5 of the ribose ring instead of the sulfur group in the more

common substrate MTA, so when attempting to model this functional group into the crystal structure the bulky aromatic ring has to be taken into account. Aromatic rings tend to be preferentially stabilized through  $\pi$ - $\pi$  stacking with another aromatic ring. In the crystal structure, two such interactions would be possible with phenylalanine moieties near the empty groove leading to the active site: Phe108 and Phe209. Interestingly, one of these residues is located on the interacting loop of the other subunit (Fig. 6*b*). This loop may therefore not only be important for dimerization but might also serve as part of the binding site, enabling the futalosine substrate to bind.

The crystal structure of the D199N mutant provides an explanation for the activity observed in the  $^1\text{H}$  NMR activity experiments. The slight activity observed in these experiments is proposed to be caused by spontaneous hydrolysis after ligand binding. The mutant is able to bind the substrate, but the asparagine is unable to bind the adenine moiety tightly enough for full hydrolysis to occur. The structure and activity data together provide evidence that HpyMqnB and arguably futalosine hydrolases in general follow the same mechanism as proposed for MTANs. The mutant crystal structure shows the importance of the acidic residue Asp199 in the hydrolysis process; without the donation of its H atom, the bond between the adenine and ribose moieties is rendered less susceptible to nucleophilic attack. The other residue chosen for mutation, Glu14, serves an equally critical role by activating a water molecule. The activity experiments show that mutating the glutamic acid to an alanine residue totally abolishes activity, whilst when the active site is kept intact (E14Q) there is still some residual activity. This could be explained by either spontaneous attack by a water molecule or by another residue (Glu176 at 3.4 Å) helping to activate the water molecule.

### 4.2. Implications for the futalosine pathway

When comparing divergence in the futalosine pathway in terms of substrate, the adenine moiety is equivalent to an inosine group in the substrates of the *H. pylori* enzyme and the *S. coelicolor* homologue, respectively. Interestingly, the catalytic residue (Asp199 in HpyMqnB) is equivalent to an asparagine in the *S. coelicolor* homologue (Fig. 2). Whether this difference is responsible for the variation in substrate remains to be investigated. The inability of the D199N mutant to process 6-amino-6-deoxyfutalosine is compatible with the fact that the *S. coelicolor* homologue can only process futalosine and not the *H. pylori* enzyme substrate (Arakawa *et al.*, 2011). Further analysis of the structure and comparison with *E. coli* homologue structures will also aid in the development of therapeutic applications. Essential residues that enable HpyMqnB to process 6-amino-6-deoxyfutalosine but are lacking in other species can provide important clues in the search for specific inhibitors, which have recently been described (Wang *et al.*, 2012). The structures reported here provide further evidence for the basis of the substrate specificity of the enzyme and can therefore be used, alongside other

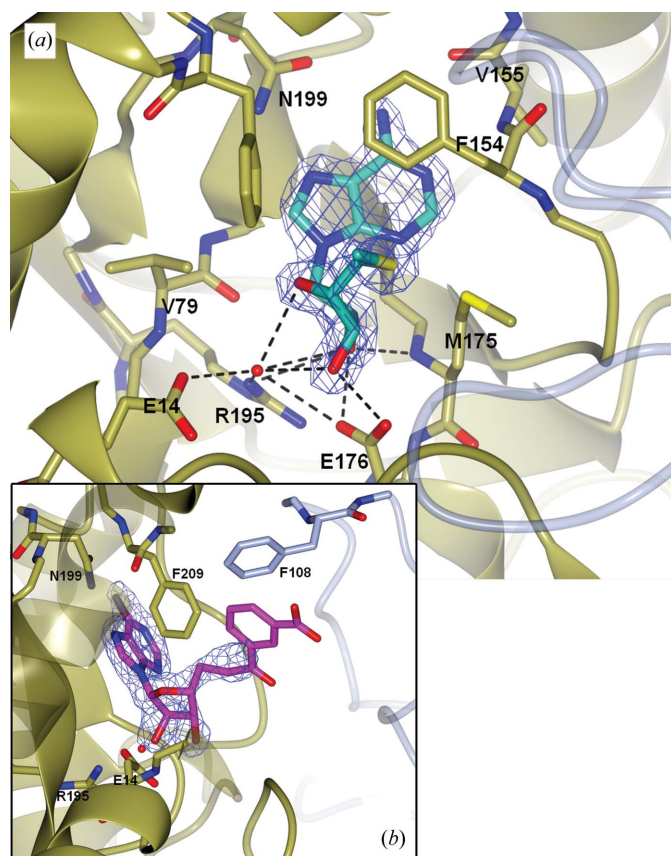


**Figure 6**

The structure of the active-site mutant D199N shows a methylthioadenosine molecule in the active site (*a*). In contrast to the wild-type structure, in the crystal structure of the D199N mutant both subunits of the dimer are in the ligand-bound form and show an intermediate state in the enzymatic reaction. The structure can be used to model the futalosine substrate (in purple) into the active site (*b*) to identify other important interacting residues.

MTAN structures, as templates for drug design targeting the futasolone pathway of *H. pylori*.

This work was carried out with the support of the Diamond Light Source. KAS thanks the Australian Research Council for funding. Furthermore, thanks are extended to Matthias Bechmann and Jen Potts (University of York) for their help with the  $^1\text{H}$  NMR spectroscopy experiments.

## References

- Albers, E. (2009). *IUBMB Life*, **61**, 1132–1142.
- Arakawa, C., Kuratsu, M., Furihata, K., Hiratsuka, T., Itoh, N., Seto, H. & Dairi, T. (2011). *Antimicrob. Agents Chemother.* **55**, 913–916.
- Baskaran, N., Kandpal, R. P., Bhargava, A. K., Glynn, M. W., Bale, A. & Weissman, S. M. (1996). *Genome Res.* **6**, 633–638.
- Bentley, R. & Meganathan, R. (1982). *Microbiol. Rev.* **46**, 241–280.
- Borodina, I., Krabben, P. & Nielsen, J. (2005). *Genome Res.* **15**, 820–829.
- Emsley, P., Lohkamp, B., Scott, W. G. & Cowtan, K. (2010). *Acta Cryst.* **D66**, 486–501.
- Glasner, M. E., Fayazmanesh, N., Chiang, R. A., Sakai, A., Jacobson, M. P., Gerlt, J. A. & Babbitt, P. C. (2006). *J. Mol. Biol.* **360**, 228–250.
- Gloster, T. M. & Davies, G. J. (2010). *Org. Biomol. Chem.* **8**, 305–320.
- Gouet, P., Robert, X. & Courcelle, E. (2003). *Nucleic Acids Res.* **31**, 3320–3323.
- Hiratsuka, T., Furihata, K., Ishikawa, J., Yamashita, H., Itoh, N., Seto, H. & Dairi, T. (2008). *Science*, **321**, 1670–1673.
- Hiratsuka, T., Itoh, N., Seto, H. & Dairi, T. (2009). *Biosci. Biotechnol. Biochem.* **73**, 1137–1141.
- Joosten, R. P., Joosten, K., Murshudov, G. N. & Perrakis, A. (2012). *Acta Cryst.* **D68**, 484–496.
- Kabsch, W. (2010). *Acta Cryst.* **D66**, 125–132.
- Kohanski, M. A., Dwyer, D. J. & Collins, J. J. (2010). *Nature Rev. Microbiol.* **8**, 423–435.
- Krissinel, E. & Henrick, K. (2007). *J. Mol. Biol.* **372**, 774–797.
- Kurosu, M. & Begari, E. (2010). *Molecules*, **15**, 1531–1553.
- Lee, J. E., Cornell, K. A., Riscoe, M. K. & Howell, P. L. (2001a). *Acta Cryst.* **D57**, 150–152.
- Lee, J. E., Cornell, K. A., Riscoe, M. K. & Howell, P. L. (2001b). *Structure*, **9**, 941–953.
- Lee, J. E., Cornell, K. A., Riscoe, M. K. & Howell, P. L. (2003). *J. Biol. Chem.* **278**, 8761–8770.
- Lee, J. E., Singh, V., Evans, G. B., Tyler, P. C., Furneaux, R. H., Cornell, K. A., Riscoe, M. K., Schramm, V. L. & Howell, P. L. (2005). *J. Biol. Chem.* **280**, 18274–18282.
- Lee, J. E., Smith, G. D., Horvatin, C., Huang, D. J. T., Cornell, K. A., Riscoe, M. K. & Howell, P. L. (2005). *J. Mol. Biol.* **352**, 559–574.
- Leslie, A. G. W. & Powell, H. R. (2007). *Evolving Methods for Macromolecular Crystallography*, edited by R. J. Read & J. L. Sussman, pp. 41–51. Dordrecht: Springer.
- Li, X., Apel, D., Gaynor, E. C. & Tanner, M. E. (2011). *J. Biol. Chem.* **286**, 19392–19398.
- Liu, H. & Naismith, J. H. (2008). *BMC Biotechnol.* **8**, 91.
- McNicholas, S., Potterton, E., Wilson, K. S. & Noble, M. E. M. (2011). *Acta Cryst.* **D67**, 386–394.
- Murshudov, G. N., Skubák, P., Lebedev, A. A., Pannu, N. S., Steiner, R. A., Nicholls, R. A., Winn, M. D., Long, F. & Vagin, A. A. (2011). *Acta Cryst.* **D67**, 355–367.
- Nathan, C. (2004). *Nature (London)*, **431**, 899–902.
- Ronning, D. R., Iacopelli, N. M. & Mishra, V. (2010). *Protein Sci.* **19**, 2498–2510.
- Seto, H., Jinnai, Y., Hiratsuka, T., Fukawa, M., Furihata, K., Itoh, N. & Dairi, T. (2008). *J. Am. Chem. Soc.* **130**, 5614–5615.
- Singh, V., Evans, G. B., Lenz, D. H., Mason, J. M., Clinch, K., Mee, S., Painter, G. F., Tyler, P. C., Furneaux, R. H., Lee, J. E., Howell, P. L. & Schramm, V. L. (2005). *J. Biol. Chem.* **280**, 18265–18273.
- Siu, K. K. W., Lee, J. E., Smith, G. D., Horvatin-Mrakovcic, C. & Howell, P. L. (2008). *Acta Cryst.* **F64**, 343–350.
- Siu, K. K. W., Lee, J. E., Sufrin, J. R., Moffatt, B. A., McMillan, M., Cornell, K. A., Isom, C. & Howell, P. L. (2008). *J. Mol. Biol.* **378**, 112–128.
- Sommer, M. O. A. & Dantas, G. (2011). *Curr. Opin. Microbiol.* **14**, 556–563.
- Suttie, J. W. (1995). *Annu. Rev. Nutr.* **15**, 399–417.
- Tanaka, R., Kunisada, T., Kushida, N., Yamada, K., Ikeda, S., Noike, M., Ono, Y., Itoh, N., Takami, H., Seto, H. & Dairi, T. (2011). *J. Antibiot.* **64**, 151–153.
- Vagin, A. & Teplyakov, A. (2010). *Acta Cryst.* **D66**, 22–25.
- Walsh, C. (2003). *Nature Rev. Microbiol.* **1**, 65–70.
- Wang, S., Haapalainen, A. M., Yan, F., Du, Q., Tyler, P. C., Evans, G. B., Rinaldo-Matthis, A., Brown, R. L., Norris, G. E., Almo, S. C. & Schramm, V. L. (2012). *Biochemistry*, **51**, 6892–6894.
- Winn, M. D. *et al.* (2011). *Acta Cryst.* **D67**, 235–242.
- Zhao, G., Wan, W., Mansouri, S., Alfaro, J. F., Bassler, B. L., Cornell, K. A. & Zhou, Z. S. (2003). *Bioorg. Med. Chem. Lett.* **13**, 3897–3900.